

# DATA ASSIMILATION IN 2D NONLINEAR COUPLED SOUND AND HEAT FLOW, USING A STABILIZED EXPLICIT FINITE DIFFERENCE SCHEME MARCHED BACKWARD IN TIME.

ALFRED S. CARASSO\*

**Abstract.** This paper considers the ill-posed data assimilation problem associated with hyperbolic/parabolic systems describing 2D coupled sound and heat flow. Given hypothetical data at time  $T > 0$ , that *may not* correspond to an actual solution of the dissipative system at time  $T$ , initial data at time  $t = 0$  are sought that can evolve, through the dissipative system, into a useful approximation to the desired data at time  $T$ . That *may not* always be possible. A stabilized *explicit* finite difference scheme, marching backward in time, is developed and applied to nonlinear examples in non rectangular regions. Stabilization is achieved by applying a compensating smoothing operator at each time step, to quench the instability. Analysis of convergence is restricted to the transparent case of linear, autonomous, selfadjoint spatial differential operators. However, the actual computational scheme can be applied to more general problems. Data assimilation is illustrated using  $512 \times 512$  pixel images. Such images are associated with highly irregular non smooth intensity data that severely challenge ill-posed reconstruction procedures. Successful and unsuccessful examples are presented.

**Key words.** Coupled sound and heat flow backward in time; stabilized explicit marching schemes; error bounds; numerical experiments.

**AMS subject classifications.** 35L15, 35K15, 35R25, 65N12, 65N21.

**1. Introduction.** As was the case in [1–4], the present paper considers the *data assimilation* problem of recreating plausible initial values at  $t = 0$ , given *hypothetical* and/or *partially known* data at some later time  $T > 0$ , in a coupled hyperbolic/parabolic system involving ill-posed time-reversed 2D coupled sound and heat flow, [5–8]. A particularly advantageous direct, non iterative, *explicit*, backward marching finite difference scheme, is constructed and explored. There is considerable interest in data assimilation in the geophysical sciences [9–26], where such problems are most often treated using iterative algorithms that may include neural networks coupled with machine learning. The direct methods discussed here may provide useful initial solutions that might be further refined by such iterative procedures. Additionally, similar direct methods may be developed in specific geophysical contexts, and these can be used, when needed, to provide confirmation of unexpected results obtained by artificial intelligence methods.

Here, as was emphasized in [1–4], the given hypothetical data at time  $T > 0$  may not be smooth, *may not correspond* to an actual solution at time  $T$ , and may differ from such a solution by an *unknown large*  $\delta > 0$  in an appropriate  $\mathcal{L}^p$  norm. Moreover, it *may not be possible* to locate initial values that can evolve into a useful approximation to the desired data at time  $T$ . The above data assimilation problem differs fundamentally from the ill-posed *backward recovery* problems discussed in [27–34], where the given data at time  $T > 0$  are noisy, but relatively smooth, and are known to approximate an *actual solution* at time  $T$ , to within a *known small*  $\delta > 0$ , in an appropriate  $\mathcal{L}^p$  norm. For ill-posed initial value problems, all consistent stepwise marching schemes, whether explicit or implicit, are necessarily unconditionally unstable and lead to explosive error growth, [5, p. 59]. Nevertheless, it is possible to stabilize such schemes by applying an appropriate compensating smoothing operator at each time step to quench the instability. In [27–34], such stabilized backward marching

---

\*Applied and Computational Mathematics Division, National Institute of Standards and Technology, Gaithersburg, MD 20899. (alfred.carasso@nist.gov).

# IMAGES ARE DEFINED BY HIGHLY NON SMOOTH INTENSITY DATA THAT CHALLENGE ILL-POSED RECOVERY METHODS

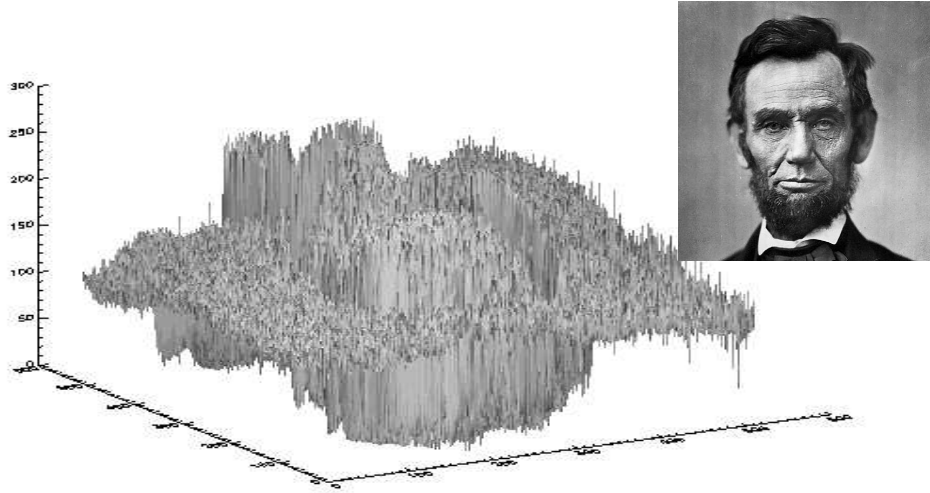


FIG. 1.1. FIGURE 1. Non smooth intensity data plot, associated with Abraham Lincoln image, is typical of many natural images.

explicit schemes have been successfully applied in backward recovery problems, and on time intervals  $[0, T]$  that are significantly larger than might be expected, based on the uncertainty estimates in [35–42]. As will be seen in Section 2.1 below, the data assimilation problem presents additional difficulties. However, limited success is still feasible in that problem, using backward marching stabilized explicit schemes.

A particularly effective vehicle for computational exploration of the proposed direct explicit data assimilation approach, lies in the use of 8 bit grey scale  $512 \times 512$  pixel images, as hypothetical data at time  $T > 0$ . As shown in Figure 1, many natural images are defined by highly non smooth intensity data that severely challenge ill-posed reconstructions. In the experiments to be described below, three such non smooth images are involved, and they interact with each other as the evolution progresses.

**2. A stabilized explicit scheme for linear selfadjoint time-reversed coupled wave and diffusion equations.** Let  $\Omega$  be a bounded domain in  $R^n$  with a smooth boundary  $\partial\Omega$ . Let  $\langle \cdot, \cdot \rangle$  and  $\| \cdot \|_2$ , respectively denote the scalar product and norm on  $\mathcal{L}^2(\Omega)$ . Let  $L$  denote a linear, second order, *positive definite* selfadjoint variable coefficient elliptic differential operator in  $\Omega$ , with homogeneous Dirichlet boundary conditions on  $\partial\Omega$ . Let  $\{\phi_m\}_{m=1}^\infty$  be the complete set of orthonormal eigenfunctions for  $L$  on  $\Omega$ , and let  $\{\lambda_m\}_{m=1}^\infty$ , satisfying

$$0 < \lambda_1 \leq \lambda_2 \leq \dots \leq \lambda_m \leq \dots \uparrow \infty, \quad (2.1)$$

be the corresponding eigenvalues.

With positive constants  $a$ ,  $b$ ,  $d$ , and  $0 < t \leq T_{max}$ , consider the linear initial

value problem on  $\Omega \times (0, T_{max}]$ ,

$$\begin{aligned}
u_t &= -bLu - dv, \\
v_t &= aLu - aLw, \\
w_t &= v, \\
u(x, 0) &= f(x), \quad v(x, 0) = g(x), \quad w(x, 0) = h(x).
\end{aligned} \tag{2.2}$$

When  $L = -\Delta$ ,  $a = c^2$ ,  $b = \sigma$ ,  $d = (\gamma - 1)$ , the above system reduces to the linearized equations of coupled sound and heat flow discussed in [5–8], namely,  $w_{tt} = c^2\Delta w - c^2\Delta u$ ,  $u_t = \sigma\Delta u - (\gamma - 1)w_t$ , with  $w = u = 0$  on  $\partial\Omega$ , where  $c$  is the isothermal sound speed,  $\sigma$  is the thermal conductivity, and  $1 < \gamma < 2$ , is the ratio of specific heats.

The initial value problem Eq. (2.2) becomes ill-posed when the time direction is reversed. We contemplate such time-reversed computations by allowing for possible *negative* time steps  $\Delta t$  in the explicit difference scheme Eq.(2.7) below. With  $\lambda_m$  as in Eq. (2.1), the positive constants  $a$ ,  $b$ ,  $d$ , and the operator  $L$  as in Eq. (2.2), fix  $\omega > 0$  and  $p > 1$ . Given  $\Delta t$ , define  $\rho$ ,  $\Lambda$ ,  $Q$ ,  $\zeta_m$ ,  $q_m$ , as follows:

$$\begin{aligned}
\rho &= \{1 + d + d^2 + 2a^2 + 2b + \sqrt{2a^2 + 2b^2}\}, \quad \Lambda = \rho(I + L), \quad Q = \exp(-\omega|\Delta t|\Lambda^p), \\
\zeta_m &= \rho(1 + \lambda_m) > 1, \quad q_m = \exp(-\omega|\Delta t|(\zeta_m)^p), \quad m \geq 1.
\end{aligned} \tag{2.3}$$

Let  $G$ ,  $S$ , and  $P$ , be the following  $3 \times 3$  matrices

$$G = \begin{bmatrix} -bL & -dI & 0 \\ aL & 0 & -aL \\ 0 & I & 0 \end{bmatrix}, \quad S = \begin{bmatrix} Q & 0 & 0 \\ 0 & Q & 0 \\ 0 & 0 & Q \end{bmatrix}, \quad P = \begin{bmatrix} \Lambda^p & 0 & 0 \\ 0 & \Lambda^p & 0 \\ 0 & 0 & \Lambda^p \end{bmatrix}. \tag{2.4}$$

Let  $W$  be the three component vector  $[u, v, w]^T$ . We may rewrite Eq. (2.2) as the equivalent first order system,

$$W_t = GW, \quad 0 < t \leq T_{max}, \quad W(\cdot, 0) = [f, g, h]^T. \tag{2.5}$$

It is instructive to study the following explicit time-marching finite difference scheme for Eq.(2.5), in which only the time variable is discretized, while the space variables remain continuous. With a given positive integer  $N$ , let  $|\Delta t| = T_{max}/N$  be the time step magnitude, and let  $W^n$  denote  $W(\cdot, n\Delta t)$ ,  $n = 0, 1, \dots, N$ . If  $W(\cdot, t)$  is the unique solution of Eq.(2.5), then

$$W^{n+1} = W^n + \Delta tGW^n + \tau^n, \tag{2.6}$$

where the ‘truncation error’  $\tau^n = \frac{1}{2}(\Delta t)^2 G^2 W(\tilde{t})$ , with  $n|\Delta t| < \tilde{t} < (n+1)|\Delta t|$ . With  $G$  and  $S$  as in Eq.(2.4), let  $R$  be the linear operator  $R = S + \Delta tSG$ . We consider approximating  $W^n$  with  $U^n \equiv [u^n, v^n]^T$ , where

$$U^{n+1} = SU^n + \Delta tSGU^n \equiv RU^n, \quad n = 0, 1, \dots, (N-1), \quad U^0 = [f, g, h]^T. \tag{2.7}$$

**Remark.** While the analysis that follows assumes  $L$  to be a linear operator, the

stabilized explicit scheme can actually be used with *nonlinear* operators  $L$ , by lagging the nonlinearity at the previous time step. This is the case in the computational experiments to be discussed below.

With  $\Delta t > 0$  and the data  $U^0$  at time  $t = 0$ , the forward marching scheme in Eq.(2.7) aims to solve a well-posed problem. However, with  $\Delta t < 0$ , together with *appropriate* data  $U^0$  at time  $T_{max}$ , marching backward from  $T_{max}$  in Eq.(2.7) attempts to solve an ill-posed problem. Define the following norms for three component vectors such as  $W(\cdot, t)$  and  $U^n$ ,

$$\begin{aligned} \|W(\cdot, t)\|_2 &= \{\|u(\cdot, t)\|_2^2 + \|v(\cdot, t)\|_2^2 + \|w(\cdot, t)\|_2^2\}^{1/2}, \\ \|U^n\|_2 &= \{\|u^n\|_2^2 + \|v^n\|_2^2 + \|w^n\|_2^2\}^{1/2}, \\ \|W\|_{2,\infty} &= \sup_{0 \leq t \leq T_{max}} \{\|W(\cdot, t)\|_2\}. \end{aligned} \quad (2.8)$$

LEMMA 1. *With  $p > 1$ , and  $\zeta_m, q_m$ , as in Eq. (2.3), fix a positive integer  $J$ , and choose  $\omega \geq (\zeta_J)^{1-p}$ . Then,*

$$q_m (1 + |\Delta t| \zeta_m) \leq 1 + |\Delta t| \zeta_J, \quad m \geq 1. \quad (2.9)$$

*Proof* : See [31, Lemma 6].

LEMMA 2. *With  $\omega, p, \zeta_J$ , as in Lemma 1, and  $R$  as in Eq.(2.7), we have  $\|R\|_2 \leq 1 + |\Delta t| \zeta_J$ . The explicit scheme in Eq.(2.7) is unconditionally stable, and*

$$\|U^n\|_2 = \|R^n U^0\|_2 \leq \exp\{n|\Delta t| \zeta_J\} \|U^0\|_2, \quad n = 1, 2, \dots, N. \quad (2.10)$$

*Proof* : See [31, Lemma 7].

LEMMA 3. *Let  $W(t)$  be the unique solution of Eq.(2.5). Then, with  $G, S$  and  $P$  as in Eq.(2.4), the definitions of the norms in Eq.(2.8), and  $0 \leq n \leq N$ ,*

$$\begin{aligned} \|\tau^n\|_2 &\leq 1/2(\Delta t)^2 \|G^2 W\|_{2,\infty}, \\ \|W^n - SW^n\|_2 &\leq \omega |\Delta t| \|PW\|_{2,\infty}, \\ |\Delta t| \|GW^n - SGW^n\|_2 &\leq \omega (\Delta t)^2 \|PGW\|_{2,\infty}. \end{aligned} \quad (2.11)$$

*Proof* : See [31, Lemma 3].

THEOREM 1. *With  $\Delta t > 0$ , let  $W^n$  be the unique solution of Eq. (2.5) at  $t = n\Delta t$ . Let  $U^n$  be the corresponding solution of the forward explicit scheme in Eq. (2.7), and let  $p, \zeta_J, \omega$ , be as in Lemma 1. If  $ER(t) \equiv U^n - W^n$ , denotes the error at  $t = n\Delta t$ ,  $n = 0, 1, 2, \dots, N$ , we have*

$$\begin{aligned} \|ER(t)\|_2 &\leq e^{t\zeta_J} \|ER(0)\|_2 + \{\omega(e^{t\zeta_J} - 1)/\zeta_J\} \|PW\|_{2,\infty} \\ &+ \{(e^{t\zeta_J} - 1)/\zeta_J\} \{\omega \Delta t \|PGW\|_{2,\infty} + (\Delta t/2) \|G^2 W\|_{2,\infty}\}. \end{aligned} \quad (2.12)$$

*Proof* : See [31, Theorem 1].

In the above forward problem, as  $\Delta t \downarrow 0$ , we are left with the error  $e^{t\zeta_J} \|ER(0)\|_2$ , originating in possibly erroneous initial data, together with the *stabilization penalty*, represented by the second term in Eq. (2.12). These errors grow monotonically as  $t$  increases. If  $T_{max}$  is large, the accumulated distortion may become unacceptably large as  $t \uparrow T_{max}$ , and the stabilized explicit scheme is not useful in that case.

Marching backward from  $t = T_{max}$  in the backward problem, solutions exist only for a restricted class of data satisfying certain smoothness constraints. Such data are seldom known with sufficient accuracy. This is especially true of the hypothetical data  $W^*(\cdot, T_{max})$  in the present data assimilation problem. It will be assumed that the given data  $U_b = W^*(\cdot, T_{max})$ , differ from the necessary exact data  $W(\cdot, T_{max})$ , by an *unknown* amount  $\delta$  in the  $\mathcal{L}^2(\Omega)$  norm.

$$\|U_b - W(\cdot, T_{max})\|_2 \leq \delta. \quad (2.13)$$

This leads to the following result, as proved in [31, Theorem 2].

**THEOREM 2.** *With  $\Delta t < 0$ , let  $W^n$  be the unique solution of the forward well-posed problem in Eq. (2.5) at  $s = T_{max} - n|\Delta t|$ . Let  $U^n$  be the solution of the backward explicit scheme in Eq. (2.7), with initial data  $U(0) = U_b = [f_b, g_b, h_b]$  as in Eq.(2.13). Let  $p, \zeta_J, \omega$ , be as in Lemma 6. If  $ER(s) \equiv U^n - W^n$ , denotes the error at  $s = T_{max} - n|\Delta t|$ ,  $n = 0, 1, 2, \dots, N$ , then*

$$\begin{aligned} & \|ER(s)\|_2 \leq \delta e^{n|\Delta t|\zeta_J} + \left\{ \omega(e^{n|\Delta t|\zeta_J} - 1)/\zeta_J \right\} \|PW\|_{2,\infty} \\ & + \left\{ (e^{n|\Delta t|\zeta_J} - 1)/\zeta_J \right\} \left\{ \omega|\Delta t| \|PGW\|_{2,\infty} + (|\Delta t|/2) \|G^2W\|_{2,\infty} \right\}. \end{aligned} \quad (2.14)$$

**2.1. Application to data assimilation.** In Theorems 1 and 2 above, define the constants  $K_1$  through  $K_5$  as follows, and consider the values shown in Table 1 below.

$$\begin{aligned} K_1 &= e^{\zeta_J T_{max}}, \quad K_2 = \omega(e^{\zeta_J T_{max}} - 1)/\zeta_J, \quad K_3 = |\Delta t|K_2, \quad K_4 = K_3/(2\omega), \\ K_5 &= K_2 \|PW\|_{2,\infty} + K_3 \|PGW\|_{2,\infty} + K_4 \|G^2W\|_{2,\infty}. \end{aligned} \quad (2.15)$$

TABLE 1

Values of  $K_1$  through  $K_4$  in Eq. (2.15), with following parameter values:  
 $T_{max} = 1.6 \times 10^{-4}$ ,  $|\Delta t| = (4/3) \times 10^{-7}$ ,  $p = 3.35$ ,  $\zeta_J = 19800$ ,  $\omega = \zeta_J^{(1-p)} = 8 \times 10^{-11}$ .

$K_1 = e^{\zeta_J T_{max}}$	$K_2 = (\zeta_J)^{-p}(K_1 - 1)$	$K_3 =  \Delta t K_2$	$K_4 = K_3/(2\omega)$
$K_1 < 23.8$	$K_2 < 9.2 \times 10^{-14}$	$K_3 < 1.3 \times 10^{-20}$	$K_4 < 7.7 \times 10^{-11}$

As outlined in the Introduction, data assimilation applied to the system in Eq. (2.5), is the problem of finding initial values  $[u(\cdot, 0), v(\cdot, 0), w(\cdot, 0)]$ , at  $t = 0$ , that can evolve into useful approximations to  $W^*(\cdot, T_{max})$ , the given hypothetical data at an appropriate time  $T_{max} > 0$ . If the true solution in Eq. (2.5) does not have exceedingly large values for  $\|PW\|_{2,\infty}$ ,  $\|PGW\|_{2,\infty}$ , or  $\|G^2W\|_{2,\infty}$ , the parameter values chosen

in Table 1, together with Theorem 2, indicate that marching backward to time  $t = 0$  from the hypothetical data  $W^*$  at  $T_{max}$ , leads to an error  $ER(0)$ , satisfying

$$\| ER(0) \|_2 \leq \delta K_1 + K_5, \quad (2.16)$$

where the constant  $K_5$  may be negligible compared to  $\delta K_1$ . Next, from Theorem 1, marching forward to time  $T_{max}$  using the inexact computed initial values  $U(\cdot, 0)$ , leads to an error  $ER(T_{max})$ , satisfying

$$\| ER(T_{max}) \|_2 \leq K_1(\delta K_1 + K_5) + K_5. \quad (2.17)$$

The error  $ER(T_{max})$  in Theorem 1 is the difference at time  $T_{max}$ , between the unknown unique solution  $W(\cdot, t)$  in Eq.(2.5), and the computed numerical approximation to it,  $U(\cdot, t)$ , provided by the stabilized forward explicit scheme. However,  $\| W^*(\cdot, T_{max}) - W(\cdot, T_{max}) \|_2 \leq \delta$ , if  $W^*(\cdot, T_{max})$  is the given hypothetical data. Hence, using the triangle inequality, one finds

$$\| W^*(\cdot, T_{max}) - U(\cdot, T_{max}) \|_2 \leq \delta(1 + K_1^2) + K_5(1 + K_1). \quad (2.18)$$

Therefore, data assimilation is successful only if the inexact computed initial values  $U(\cdot, 0)$  at  $t = 0$ , lead to a sufficiently small right hand side in Eq.(2.18). Clearly, the value of  $\zeta_J T_{max}$ , together with the unknown value of  $\delta$ , will play a vital role. From Table 1, we find  $\delta(1 + K_1^2) < 568 \delta$ . However, with  $T_{max}$  chosen five times larger, one would find  $\delta(1 + K_1^2) > (5.8 \times 10^{13}) \delta$ .

**2.2. Using the Laplacian for smoothing when  $L$  has variable coefficients.** All of the discussion and results in [31, Section 6] on using the Laplacian for smoothing, can be applied to the linear system in Eq. (2.5). With  $\rho$ ,  $\Lambda$ ,  $Q$  as in Eq. (2.3), let  $\Gamma = \rho(I - \Delta)$ . For real  $q > 1$ , and  $\epsilon > 0$ , define  $Q_\Delta = \exp\{-\epsilon|\Delta t|\Gamma^q\}$ . In domains where closed form expressions for the eigenfunctions of the Laplacian are known, it may be advantageous to use the smoothing operator  $Q_\Delta$  in lieu of  $Q$  in the stabilized explicit scheme in Eq. (2.7). This is feasible for differential operators  $L$  where the hypothesis in [31, Eq. (6.2)] is valid, so that, with appropriately chosen  $(\epsilon, q)$ , one has  $\| Q_\Delta g \|_2 \leq \| Qg \|_2$ , for all  $g \in \mathcal{L}^2(\Omega)$  and sufficiently small  $|\Delta t|$ . When this is the case, Theorems 1 and 2 remain valid, with  $S_\Delta$  and  $P_\Delta$  replacing  $S$  and  $P$ . Moreover, as described in [31, Section 6.1], and as will be demonstrated in the computational experiments discussed below, it may be possible to use efficient FFT algorithms to synthesize  $Q_\Delta$ , even in problems defined on non-rectangular domains  $\Omega$ .

**3. Data assimilation in nonlinear coupled sound and heat flow in non-rectangular region, using FFT Laplacian smoothing.** We now highlight the versatility of the stabilized scheme in Eq. (2.7), by considering a nonlinear example in a non-rectangular region, in which the explicit computation proceeds by lagging the nonlinearity at the previous time step. Let  $\Omega$  be the open quarter circle region in the  $(x, y)$  plane,

$$0.05 < x, y < 0.95, \quad (x - 0.05)^2 + (y - 0.05)^2 < (0.9)^2, \quad (3.1)$$

let  $T_{max} = 1.6 \times 10^{-4}$ , and let  $L$  be the nonlinear differential operator defined as follows on functions  $z(x, y, t)$  on  $\Omega \times (0, T_{max})$ :

$$Lz = -0.00085 s(z) \nabla \cdot \{q(x, y) \nabla z\} - 2.75(z_x + z_y), \quad (3.2)$$

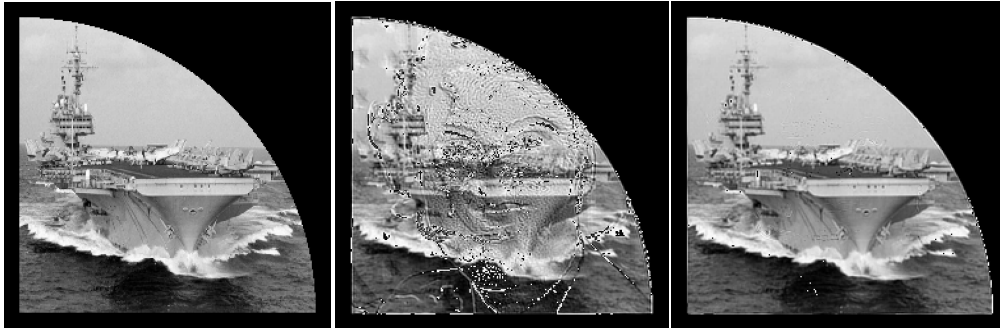
SUCCESSFUL DATA ASSIMILATION FROM  $T=1.6E-4$ .

U=Temperature, V=wave velocity, W=wave displacement.

Desired U at time T    Computed U at t=0    Evolved U at time T



Desired V at time T    Computed V at t=0    Evolved V at time T



Desired W at time T    Computed W at t=0    Evolved W at time T



FIG. 3.1. FIGURE 2. Successful data assimilation experiment. See summary in Table 2. Above nonlinear coupled sound and heat flow experiment lies outside scope of linear theory developed in Section 2. As explained in the discussion following Eq. (3.4), enclosing quarter circle region  $\Omega$  in unit square  $\Psi$ , allows use of FFT Laplacian smoothing operator  $Q_{\Delta}$ , in backward reconstruction with scheme in Eq. (2.7).

UNSUCCESSFUL DATA ASSIMILATION FROM  $T = 8.0 \text{ E-4}$ .

U=Temperature, V=wave velocity, W=wave displacement.

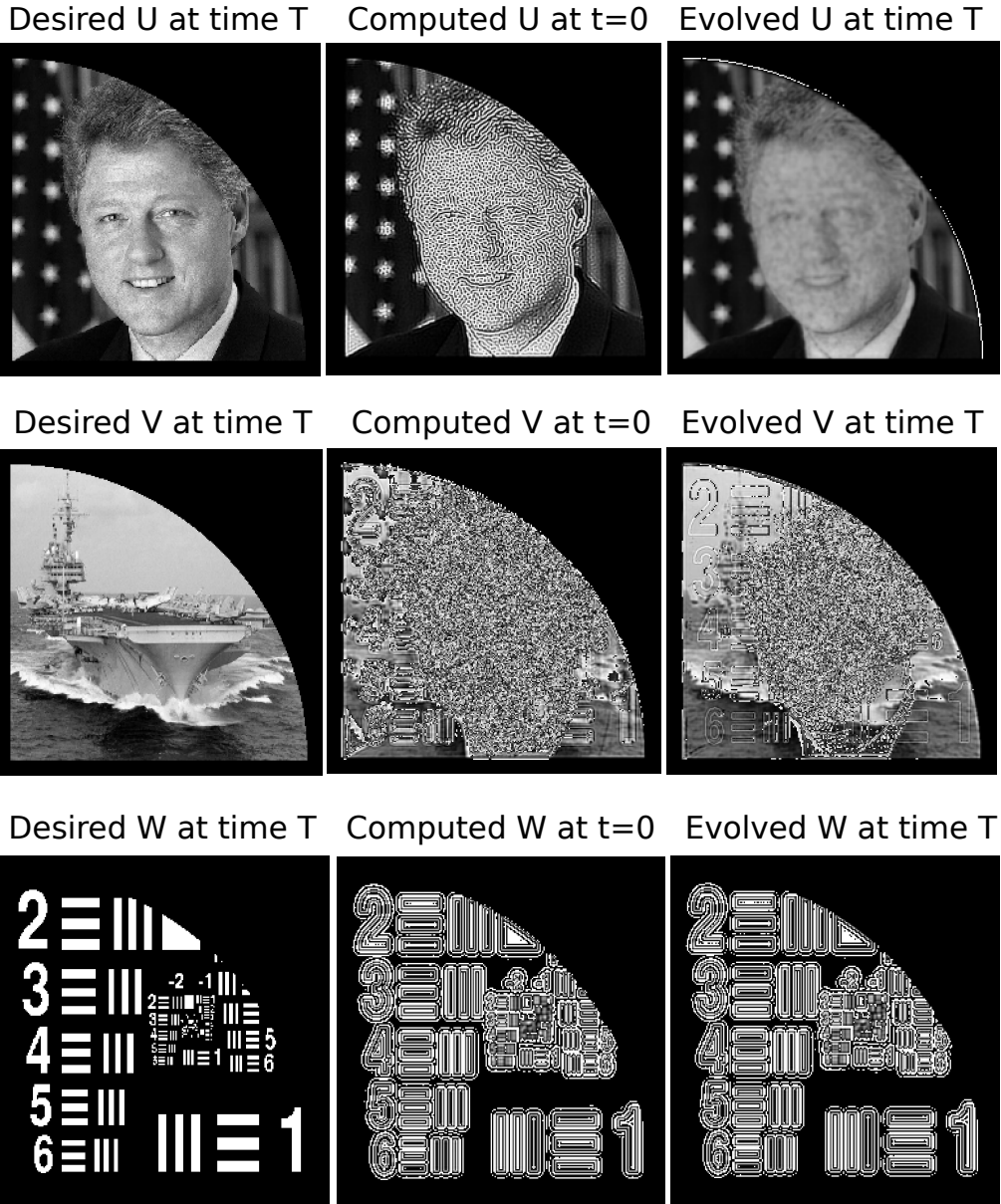


FIG. 3.2. FIGURE 3. Failure of data assimilation with significantly larger value for  $T_{max}$ . See summary in Table 3. As previously explained, enclosing quarter circle region  $\Omega$  in unit square  $\Psi$ , allows use of FFT Laplacian smoothing operator  $Q_{\Delta}$ , in backward reconstruction with scheme in Eq. (2.7).



where

$$s(z) = \exp\{0.005z\}, \quad 1 < q(x, y) = \{1 + 2 \sin \pi x \sin \pi y\} \leq 3, \quad (3.3)$$

With  $a = 6$ ,  $b = 5$ ,  $d = 0.95$ , and  $(x, y, t) \in \Omega \times (0, T_{max})$ , consider the system

$$\begin{aligned} u_t &= -bLu - dv, \\ v_t &= aLu - aLw, \\ w_t &= v, \\ u(x, y, T_{max}) &= f(x, y), \quad v(x, y, T_{max}) = g(x, y), \quad w(x, y, T_{max}) = h(x, y), \\ u(x, y, t) &= v(x, y, t) = w(x, y, t) = 0, \quad (x, y, t) \in \partial\Omega \times [0, T_{max}]. \end{aligned} \quad (3.4)$$

In Eq. (3.4),  $u(x, y, t)$  denotes the temperature,  $w(x, y, t)$  is the wave displacement, and  $v = w_t(x, y, t)$  is the wave velocity. The hypothetical data at time  $T_{max}$ , namely,  $f(x, y)$ ,  $h(x, y)$ ,  $g(x, y)$ , are the three images shown in the leftmost column in Figure 2. Here, the quarter circle region  $\Omega$  was enclosed in the unit square  $\Psi = \{0 < x, y < 1\}$ . A  $512 \times 512$  uniform grid was imposed on  $\Psi$ , leading to a discrete boundary  $\partial\Omega_d$  consisting of the grid points closest to  $\partial\Omega$ . This was assumed to sufficiently well-approximate  $\partial\Omega$ . With  $\Delta x = \Delta y = 1/512$ , and  $\Delta t = -(4/3) \times 10^{-7}$ , homogeneous boundary conditions were applied on  $\partial\Omega_d$ . Lagging the nonlinearity at the previous time step, explicit time differencing together with centered finite differencing in the space variables, were used in the *stabilized backward computation*, as described below, for  $1200 \Delta t$ . This produced the images at  $t = 0$ , shown in the middle column in Figure 2. The actual computed data at  $t = 0$  involve negative values. These values are not used in forming and displaying the middle column images, but are nevertheless retained as necessary to enable computation of the images in the rightmost column in Figure 2.

With  $\rho$  as in Eq. (2.3),  $\Gamma = \rho(I - \Delta)$ , real  $q > 1$ , and  $\epsilon > 0$ , let  $Q_\Delta = \exp\{-\epsilon|\Delta t|\Gamma^q\}$ . In the above stabilized backward computation at each time step  $m$  in Eq. (2.7), after applying the operator  $(I + \Delta tG)$  to  $U^m$  on  $\Omega \subset \Psi$ , the solution is extended to all of  $\Psi$  by defining it to be zero on  $\Psi - \Omega$ . FFT algorithms are then applied on  $\Psi$  to synthesize  $Q_\Delta$ , and produce  $U^{m+1} = S_\Delta(I + \Delta tG)U^m$ , while retaining only the values of  $U^{m+1}$  on  $\Omega$ . This process is then repeated at the next time step. Interactive trials are needed to locate appropriate values for  $(\epsilon, q)$ . Here, a parameter pair  $\epsilon = 8.0 \times 10^{-11}$ ,  $q = 3.35$ , was arrived at after very few trials.

As is evident from Figure 2, together with the accompanying data in Table 2, data assimilation was successful in that computational experiment. At time  $T_{max}$ , the evolved  $L^1$  norms closely match the desired  $L^1$  norms, and the resulting  $L^1$  relative errors are small. In the linear selfadjoint problem contemplated in Table 1 and Eq.(2.18), we found  $\delta(1 + K_1^2) < 568 \delta$ , when using the same parameter values that were used in the nonlinear problem in Figure 2. However, with  $T_{max}$  chosen five times larger in the linear problem, we found  $\delta(1 + K_1^2) > (5.8 \times 10^{13}) \delta$ .

We now consider data assimilation for the same nonlinear problem described in Eq. (3.4), with the same parameters used in Figure 2 and Table 2, except for  $T_{max}$ , which is now chosen *five time larger*, with the Elizabeth Taylor image replaced by the USAF 1951 resolution chart. As can be seen from Figure 3 and Table 3, data assimilation is now unsuccessful. The images in the rightmost column in Figure 3, do

not match the desired images in the leftmost column. The evolved  $L^1$  norms are not good approximations to the desired  $L^1$  norms at time  $T_{max}$ , and the accompanying  $L^1$  relative errors are quite large. While the failure in the above nonlinear experiment with  $T_{max} = 8.0 \times 10^{-4}$  is less catastrophic than was predicted in the linear selfadjoint case with the same  $T_{max}$  value, the linear analysis in Table 1 and Eq.(2.18), was a useful guide. As previously noted, successful reconstruction in backward dissipative evolution equations is necessarily limited, given the associated uncertainty estimates, in [35–42].

TABLE 2

Behavior of  $L^1$  norm in successful data assimilation example shown in Figure 2.  $T_{max} = 1.6 \times 10^{-4}$ ,  $|\Delta t| = (4/3) \times 10^{-7}$ ,  $p = 3.35$ ,  $\zeta_J = 19800$ ,  $\omega = \zeta_J^{(1-p)} = 8 \times 10^{-11}$ .

Image	Desired $L^1$ norm	Evolved $L^1$ norm	$L^1$ relative error
Bill Clinton	61.06 ( $T_{max}$ )	60.80 ( $T_{max}$ )	7.46 % ( $T_{max}$ )
USS Kitty Hawk	93.60 ( $T_{max}$ )	93.07 ( $T_{max}$ )	4.41 % ( $T_{max}$ )
Elizabeth Taylor	99.95 ( $T_{max}$ )	99.27 ( $T_{max}$ )	2.69 % ( $T_{max}$ )

TABLE 3

Behavior of  $L^1$  norm in unsuccessful data assimilation example shown in Figure 3.  $T_{max} = 8.0 \times 10^{-4}$ ,  $|\Delta t| = (4/3) \times 10^{-7}$ ,  $p = 3.35$ ,  $\zeta_J = 19800$ ,  $\omega = \zeta_J^{(1-p)} = 8 \times 10^{-11}$ .

Image	Desired $L^1$ norm	Evolved $L^1$ norm	$L^1$ relative error
Bill Clinton	61.06 ( $T_{max}$ )	56.57 ( $T_{max}$ )	18.11 % ( $T_{max}$ )
USS Kitty Hawk	93.60 ( $T_{max}$ )	85.81 ( $T_{max}$ )	48.94 % ( $T_{max}$ )
USAF chart	39.27 ( $T_{max}$ )	41.59 ( $T_{max}$ )	26.25 % ( $T_{max}$ )

**4. Concluding Remarks.** With proper parameter choices, stabilized explicit schemes appear to be helpful in difficult data assimilation problems, involving non differentiable data and nonlinear dissipative systems. Examples of failure in such problems are also instructive and valuable.

Along with [1–4], the results in the present paper invite useful scientific debate and comparisons, as to whether equally good or better results might be achieved, using the computational methods described in [9–26]. As an alternative computational approach, backward marching stabilized explicit schemes may also be helpful, if needed, in validating computations involving machine learning.

#### REFERENCES

- [1] Carasso AS. Data assimilation in 2D viscous Burgers equation using a stabilized explicit finite difference scheme run backward in time. *Inverse Probl. Sci. Eng.* 2021;29:3475–3489. DOI:10.1080/17415977.2021.200947
- [2] Carasso AS. Data assimilation in 2D nonlinear advection diffusion equations, using an explicit

- stabilized leapfrog scheme run backward in time. NIST Technical Note 2227, July 12 2022. DOI:10.6028/NIST.TN2227
- [3] Carasso AS. Data assimilation in 2D hyperbolic/parabolic systems using a stabilized explicit finite difference scheme run backward in time. *Applied Mathematics in Science and Engineering*, 2024;32:1,228641. DOI:10.1080/27690911.2023.228641
  - [4] Carasso AS. Data assimilation in 2D incompressible Navier-Stokes equations, using a stabilized explicit  $O(\Delta t)^2$  leapfrog finite difference scheme run backward in time. NIST Technical Note TN2299, August 2024. DOI:10.6028/NIST.TN2299.
  - [5] Richtmyer RD, Morton KW. *Difference Methods for Initial Value Problems*. 2nd ed. New York (NY): Wiley; 1967
  - [6] Lattès R, Lions JL. *Méthode de Quasi-Réversibilité et Applications [The Method of Quasi-Reversibility and Applications]*. Paris: Dunod; 1967.
  - [7] Lions JL. Sur l'approximation de la solution d'équations d'évolution couplées. *Rend. Mat.* 1968;1:141–176.
  - [8] Carasso AS. Coupled sound and heat flow and the method of least squares. *Math. Comp.* 1975;29:447–463.
  - [9] Cintra R, de Campos Velho HF, Cocke S. Tracking the model: data assimilation by artificial neural network. 2016 International Joint Conference on Neural Networks (IJCNN), Vancouver, BC, Canada. 2016:403-410. DOI:10.1109/IJCNN.2016.7727227.
  - [10] Howard LJ, Subramanian A, Hoteit I. A machine learning augmented data assimilation method for high resolution observations. *Journal of Advances in Modeling Earth Systems*. 2024;16,e2023MS003774. <https://doi.org/10.1029/2023MS003774>.
  - [11] Blum J, Le Dimet F-X, Navon I-M. Data Assimilation for Geophysical Fluids. *Handbook of Numerical Analysis*. 2009;14:385-441. [https://doi.org/10.1016/S1570-8659\(08\)00209-3](https://doi.org/10.1016/S1570-8659(08)00209-3)
  - [12] He Q, Barajas-Solano D, Tartakovsky G, et al. Physics-informed neural networks for multiphysics data assimilation with application to subsurface transport. *Advances in Water Resources* 2020; <https://doi.org/10.1016/j.advwatres.2020.103610>.
  - [13] Arcucci R, Zhu J, Hu S, et al. Deep data assimilation: integrating deep learning with data assimilation. *Appl. Sci.* 2021;11:1114. <https://doi.org/10.3390/app11031114>.
  - [14] Antil H, Lohner R, Price R. Data assimilation with deep neural nets informed by nudging. <https://arxiv.org/abs/2111.11505>. November 2021.
  - [15] Chen C, Dou Y, Chen J, et al. A novel neural network training framework with data assimilation. *Journal of Supercomputing*. 2022;78:19020–19045. <https://doi.org/10.1007/s11227-04629-7>
  - [16] Lundvall J, Kozlov V, Weiserfelt P. Iterative methods for data assimilation for Burgers' equation. *J. Inverse Ill-Posed Probl.* 2006;14:505–535.
  - [17] Auroux D, Blum J. A nudging-based data assimilation method for oceanographic problems: the back and forth nudging (BFN) algorithm. *Proc. Geophys.* 2008;15:305–319.
  - [18] Ou K, Jameson A. Unsteady adjoint method for the optimal control of advection and Burgers' equation using high order spectral difference method. 49th AIAA Aerospace Science Meeting, 4-7 January 2011. Orlando, Florida.
  - [19] Auroux D, Nodet M. The back and forth nudging algorithm for data assimilation problems: theoretical results on transport equations. *ESAIM:COCV* 2012;18:318–342.
  - [20] Auroux D, Bansart P, Blum J. An evolution of the back and forth nudging for geophysical data assimilation: application to Burgers equation and comparison. *Inverse Probl. Sci. Eng.* 2013;21:399-419
  - [21] Allahverdi N, Pozo A, Zuazua E. Numerical aspects of large-time optimal control of Burgers' equation. *ESAIM Mathematical Modeling and Numerical Analysis* 2016;50:1371–1401.
  - [22] Gosse L, Zuazua E. Filtered gradient algorithms for inverse design problems of one-dimensional Burgers' equation. *Innovative Algorithms and Analysis* 2017;197–227.
  - [23] de Campos Velho HF, Barbosa VCF, Cocke S. Special issue on inverse problems in geosciences. *Inverse Probl. Sci. Eng.* 2013;21:355-356. DOI:10.1080/17415977.2012.712532
  - [24] Gomez-Hernandez JJ, Xu T. Contaminant source identification in aquifers: a critical view. *Math Geosci* 2022;54:437–458.
  - [25] Xu T, Zhang W, Gomez-Hernandez JJ, et al. Non-point contaminant source identification in an aquifer using the ensemble smoother with multiple data assimilation. *Journal of Hydrology* 2022; 606:127405.
  - [26] Vukicevic T, Steyskal M, Hecht M. Properties of advection algorithms in the context of variational data assimilation. *Monthly Weather Review* 2001;129:1221–1231.
  - [27] Carasso AS. Compensating operators and stable backward in time marching in nonlinear parabolic equations. *Int J Geomath* 2014;5:1–16.
  - [28] Carasso AS. Stable explicit time-marching in well-posed or ill-posed nonlinear parabolic equa-

- tions. *Inverse Probl. Sci. Eng.* 2016;24:1364–1384.
- [29] Carasso AS. Stable explicit marching scheme in ill-posed time-reversed viscous wave equations. *Inverse Probl. Sci. Eng.* 2016;24:1454–1474.
- [30] Carasso AS. Stabilized Richardson leapfrog scheme in explicit stepwise computation of forward or backward nonlinear parabolic equations. *Inverse Probl. Sci. Eng.* 2017;25:1–24.
- [31] Carasso AS. Stabilized backward in time explicit marching schemes in the numerical computation of ill-posed time-reversed hyperbolic/parabolic systems. *Inverse Probl. Sci. Eng.* 2018;1:1–32. DOI:10.1080/17415977.2018.1446952
- [32] Carasso AS. Stable explicit stepwise marching scheme in ill-posed time-reversed 2D Burgers' equation. *Inverse Probl. Sci. Eng.* 2018;27(12):1-17. DOI:10.1080/17415977.2018.1523905
- [33] Carasso AS. Computing ill-posed time-reversed 2D Navier-Stokes equations, using a stabilized explicit finite difference scheme marching backward in time. *Inverse Probl. Sci. Eng.* 2019; DOI:10.1080/17415977.2019.1698564
- [34] Carasso AS. Stabilized leapfrog scheme run backward in time, and the explicit  $O(\Delta t)^2$  stepwise computation of ill-posed time-reversed 2D Navier-Stokes equations. *Inverse Probl. Sci. Eng.* 2021; DOI:10.1080/17415977.2021.1972997
- [35] Ames KA, Straughan B. *Non-Standard and Improperly Posed Problems*. New York (NY): Academic Press; 1997.
- [36] Payne LE. Some remarks on ill-posed problems for viscous fluids. *Int. J. Engng Sci.* 1992;30:1341–1347.
- [37] Knops RJ. Logarithmic convexity and other techniques applied to problems in continuum mechanics. In: Knops RJ, editor. *Symposium on non-well-posed problems and logarithmic convexity*. Vol. 316, *Lecture notes in mathematics*. New York (NY): Springer-Verlag; 1973.
- [38] Knops RJ, Payne LE. On the stability of solutions of the Navier-Stokes equations backward in time. *Arch. Rat. Mech. Anal.* 1968;29:331–335.
- [39] Payne LE. Uniqueness and continuous dependence criteria for the Navier-Stokes equations. *Rocky Mountain J. Math.* 1971;2:641–660.
- [40] Carasso AS. Reconstructing the past from imprecise knowledge of the present: Effective non-uniqueness in solving parabolic equations backward in time. *Math. Methods Appl. Sci.* 2012;36:249–261.
- [41] Carasso A. Computing small solutions of Burgers' equation backwards in time. *J. Math. Anal. App.* 1977;59:169–209.
- [42] Hào DN, Nguyen VD, Nguyen VT. Stability estimates for Burgers-type equations backward in time. *J. Inverse Ill Posed Probl.* 2015;23:41–49.